The intrinsically liganded cyclic nucleotide–binding homology domain promotes KCNH channel activation

Yaxian Zhao,[1,2] Marcel P. Goldschen-Ohm,[1,2] João H. Morais-Cabral,[3,4] Baron Chanda,[1,2] and Gail A. Robertson[1,2]

[1]Department of Neuroscience and [2]Cardiovascular Research Center, University of Wisconsin School of Medicine and Public Health, Madison, WI 53705

[3]Instituto de Biologia Molecular e Celular and [4]Instituto de Investigação e Inovação em Saúde, Universidade do Porto, 4150 Porto, Portugal

Channels in the ether-à-go-go or KCNH family of potassium channels are characterized by a conserved, C-terminal domain with homology to cyclic nucleotide–binding homology domains (CNBhDs). Instead of cyclic nucleotides, two amino acid residues, Y699 and L701, occupy the binding pocket, forming an "intrinsic ligand." The role of the CNBhD in KCNH channel gating is still unclear, however, and a detailed characterization of the intrinsic ligand is lacking. In this study, we show that mutating both Y699 and L701 to alanine, serine, aspartate, or glycine impairs human EAG1 channel function. These mutants slow channel activation and shift the conductance–voltage (G–V) relation to more depolarized potentials. The mutations affect activation and the G-V relation progressively, indicating that the gating machinery is sensitive to multiple conformations of the CNBhD. Substitution with glycine at both sites (GG), which eliminates the side chains that interact with the binding pocket, also reduces the ability of voltage prepulses to populate more preactivated states along the activation pathway (i.e., the Cole–Moore effect), as if stabilizing the voltage sensor in deep resting states. Notably, deletion of the entire CNBhD (577–708, ΔCNBhD) phenocopies the GG mutant, suggesting that GG is a loss-of-function mutation and the CNBhD requires an intrinsic ligand to exert its functional effects. We developed a kinetic model for both wild-type and ΔCNBhD mutant channels that describes all our observations on activation kinetics, the Cole–Moore shift, and G-V relations. These findings support a model in which the CNBhD both promotes voltage sensor activation and stabilizes the open pore. The intrinsic ligand is critical for these functional effects.

The Journal of General Physiology

INTRODUCTION

Channels in the KCNH family of potassium channels are characterized by a region of homology to cyclic nucleotide–gated channels (Fig. 1 A; Guy et al., 1991; Ganetzky et al., 1999) but are not gated by cyclic nucleotides (Robertson et al., 1996; Brelidze et al., 2009). As revealed by x-ray crystallography, they possess a fold that is strikingly similar to the binding pocket of cyclic nucleotide–binding domains (CNBDs; Zagotta et al., 2003; Clayton et al., 2004), but which instead is occupied by an "intrinsic ligand" comprising the side chains of two downstream residues that loop back to occupy the binding site (Fig. 1 B; Brelidze et al., 2012, 2013; Marques-Carvalho et al., 2012). Alanine mutations of the intrinsic ligand residues have been shown to alter membrane currents, indicating a role for the intrinsic ligand in gating (Brelidze et al., 2012, 2013; Marques-Carvalho et al., 2012; Ng et al., 2013).

Mutations in the *Drosophila melanogaster ether-à-go-go* (*eag*) gene, the founding member of the KCNH family (Warmke et al., 1991), disrupt membrane excitability and enhance transmitter release at the neuromuscular junction (Wu et al., 1983). Similarly, the mammalian orthologue of *eag*, denoted *EAG1* or *KCNH1* (Warmke and Ganetzky, 1994; Ganetzky et al., 1999), encodes a channel expressed in presynaptic terminals in the brain (Mortensen et al., 2015). Mutations in this gene have yet to be linked with neural-specific diseases but instead are known to confer growth defects associated with Zimmermann–Laband and Temple–Baraitser syndromes (Kortüm et al., 2015; Simons et al., 2015). Overexpression of human EAG1 (hEAG1) has been described in several primary cancers and is considered a biomarker for progression and invasiveness (Pardo et al., 1999; Sánchez et al., 2016).

EAG1 channels are distinguished from the closely related ERG or ELK channels by an activation process that is highly sensitive to holding or prepulse membrane potential (Ludwig et al., 1994; Robertson et al., 1996; Meyer and Heinemann, 1998; Schönherr et al., 2002). This effect, first described for potassium currents in squid axon, is characterized by slower (and in some cases more sigmoidal) current activation as holding potential is hyperpolarized (Cole and Moore, 1960). The delay in activation,

Correspondence to Gail A. Robertson: garobert@wisc.edu

Abbreviations used: CNBD, cyclic nucleotide–binding domain; CNBhD, cyclic nucleotide–binding homology domain; VSD, voltage sensor domain.

The Rockefeller University Press $30.00
J. Gen. Physiol. 2017 Vol. 149 No. 2 249–260
https://doi.org/10.1085/jgp.201611701

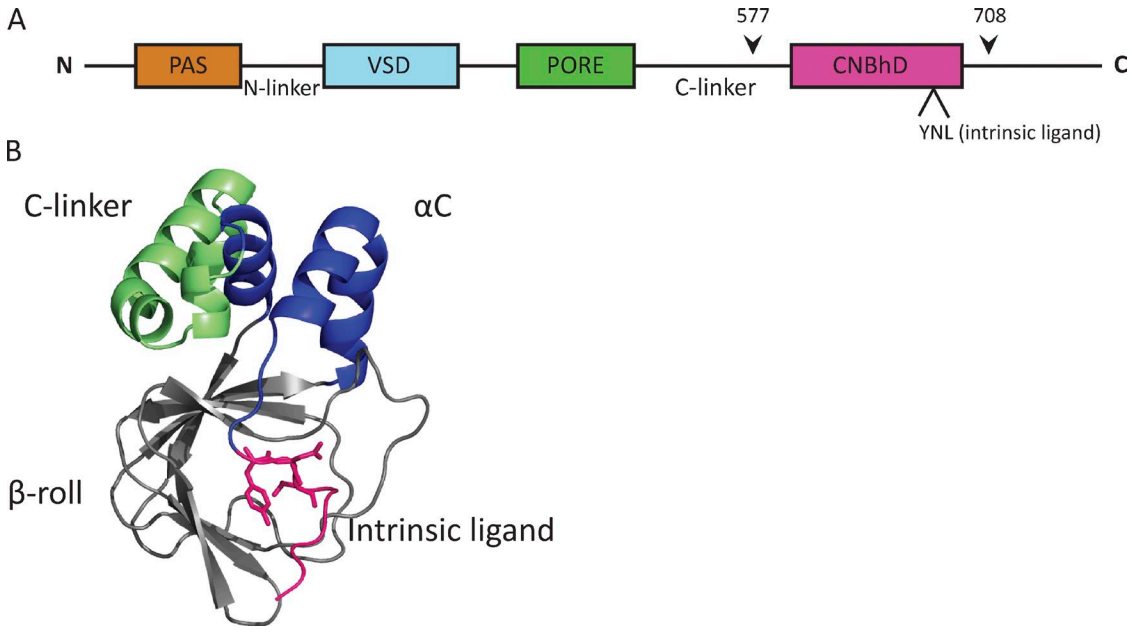

Figure 1. **Domains of hEAG1 channel and CNBHD structure.** (A) Schematic showing domains of hEAG1. Region deleted in ΔCNBhD mutant is marked by arrowheads. (B) Cartoon representation of the structure of the CNBhD from mEAG1 channel (adapted from Marques-Carvalho et al., 2012; PDB accession no. 4F8A). C-linker stretch is depicted in green, CNBhD helices are in blue, and β-roll is in gray. Residues forming the intrinsic ligand are shown in magenta.

referred to as the Cole–Moore effect, reflects the existence of multiple closed states associated with intermediate conformations of the voltage sensor domains (VSDs) that are traversed before pore opening (Cole and Moore, 1960) and associated with fractional gating charge movement (Bannister et al., 2005). The Cole–Moore effect is modular in nature, such that channels produced by combining EAG1 VSDs and ERG pore domains exhibit a prepulse sensitivity in activation kinetics not observed for WT ERG channels (Lörinczi et al., 2015).

Despite the strong similarity with cyclic nucleotide–binding domains, the role of the cyclic nucleotide–binding homology domain (CNBhD) is unclear, and detailed mechanistic studies of the intrinsic ligand are lacking. Here, we show that various mutations of the intrinsic ligand residues in hEAG1 channels impair channel activation, and removing the intrinsic ligand side chains by substitution with glycines is functionally equivalent to deleting the entire CNBhD. We developed kinetic models for both WT and ΔCNBhD mutant channels that can explain the observed current properties, including activation kinetics, the Cole–Moore shift, and G-V relations. Thus, the role of the liganded CNBhD is to promote activation of the voltage-sensing domains and stabilize the open pore.

MATERIALS AND METHODS

Molecular biology

Human *EAG1* (*hEAG1* or *KCNH1*; GenBank accession no. NM_002238.3) cDNA cloned into psGEM oocyte expression vector was a gift from R. Schonherr (Friedrich-Schiller-Universität, Jena, Germany). Mutations in WT *hEAG1* cDNA were made using the QuikChange site-directed mutagenesis kit (Agilent Technologies) and verified by DNA sequence analysis. Plasmid DNA was linearized by NheI and cRNA and transcribed in vitro with the mMessage mMachine T7 kit (Thermo Fisher Scientific).

Oocyte isolation and cRNA injection

To remove the follicle cell layer, *Xenopus laevis* oocytes were first isolated with forceps and then treated with 75 µg/ml Liberase TM research-grade enzyme (Sigma-Aldrich) for 40–60 min in Ca^{2+}-free ND96 solution that contained 96 mM NaCl, 2 mM KCl, 1 mM $MgCl_2$, and 5 mM HEPES, with pH adjusted to 7.4 with NaOH. Stage IV and V oocytes were injected with WT or mutant cRNA and incubated for 1–5 d at 16°C in storage solution before voltage-clamp experiments. Storage solution contained 96 mM NaCl, 2 mM KCl, 1.8 mM $CaCl_2$, 1 mM $MgCl_2$, 1 mM HEPES, and 10 mg/L gentamycin, with pH adjusted to 7.4 with NaOH.

Two-electrode voltage-clamp protocols and data analysis

Oocytes expressing channels of interest were subjected to a standard two-microelectrode voltage clamp. Recording solution was perfused through the bath chamber during the recording. Recording solution contained 96 mM NaCl, 2 mM KCl, 0.3 mM $CaCl_2$, 1 mM $MgCl_2$, and 5 mM HEPES, with pH adjusted to

Table 1. **Kinetic model parameters**

Transition	Symbol	WT (n = 6)		ΔCNBHD (n = 6)	
		k_0	q	k_0	q
		s^{-1}	e^-	s^{-1}	e^-
C0 → C1	α	16.3 ± 1.4	0.05	9.8 ± 1.5	0.05
C1 → C0	β	0.78 ± 0.22	−0.45	0.66 ± 0.31	−0.45
C1 → C2	γ	270 ± 135	0.60	18.8 ± 7.4	0.60
C2 → C1	δ	0.47 ± 0.3	−1.4	1.38 ± 0.4	−1.4
C2 → O	o	145 ± 70.1	NA	145	NA
O → C2	c	170 ± 52	−0.50	2,066 ± 47	−0.50
O → I	i	91 ± 49.2	0.39 ± 0.13	91	0.39
I → O	r	619 ± 402	−0.50	619	−0.50

NA, not applicable. Voltage-dependent rate constants are given by $k(V) = k_0 \exp(qV/k_BT)$, where k_0 is the voltage-independent rate, q is the effective charge moved from the initial state up to the transition state intermediate, V is voltage, k_B is Boltzmann's constant, and T is temperature (held at 298.15 K). Parameters are the mean ± SEM for models optimized to data from individual oocytes.

7.4 with NaOH. An OC-725C amplifier (Warner Instruments), Digidata 1440A data acquisition system, and pCLAMP 9.0 software (Molecular Devices) were used to produce command voltages and record current and voltage signals. The resistance of microelectrodes after breaking their tip and filling with 3 M KCl ranged from 0.2 to 0.6 MΩ.

To determine the G-V relationship, series of depolarizing potentials ranging from −100 to 80 mV were applied in 10-mV increments for 1 s from a holding potential of −80 mV. Current conductance (G) was calculated from the Goldman–Hodgkin–Katz equation (Hodgkin and Katz, 1949) by dividing the steady-state current by driving force:

$$G = \frac{I_{ss}}{GHK[V - E_K]} = \frac{I_{ss}}{\frac{FV\exp[F(V - E_K)/RT] - 1}{RT\exp(FV/RT) - 1}},$$

where I_{ss} is the steady-state current, E_K is the membrane reversal potential, F is the Faraday constant, R is the gas constant, and T is temperature. G was normalized to G_{max} and plotted as a function of depolarizing potentials. The G-V relationship was then fitted with the Boltzmann function:

$$\frac{G}{G_{max}} = \frac{1}{\left[1 + e^{-\left(\frac{V - V_{1/2}}{s}\right)}\right]},$$

where $V_{1/2}$ is the voltage of half-maximal activation and s is the slope factor. Efforts were made to derive conductance using a standard tail current method, but even under conditions of elevated external K concentration to increase tail current amplitude and lowered temperatures to slow deactivation kinetics, the tail currents remained too fast relative to the two-electrode voltage clamp settling time to be resolved.

Offline data analysis was performed with Clampfit 10.2 (Molecular Devices), Origin 9 (OriginLab), and Excel (Microsoft) software. All data are expressed as mean ± SEM (n = number of oocytes), and statistical significance was evaluated by two-way ANOVA or Student's t test where appropriate ($P \leq 0.05$ was considered a statistically significant difference).

Kinetic modeling of hEAG1 currents

Kinetic models for WT and ΔCNBHD channels were developed using Kinetic Model Builder version 2.0 (Goldschen-Ohm et al., 2014; https://sourceforge.net/projects/modbuilder). Models were simultaneously optimized by minimizing the weighted sum of squared errors between simulated and observed current responses to a wide range of voltage steps, both with and without a voltage prepulse (i.e., Cole–Moore effect), using a simplex algorithm. During each epoch (period of constant voltage), the weights at each sample point decayed exponentially to a constant value with a time constant of either 30 or 50 ms, such that current behavior immediately after a change in voltage was given precedence during optimization (this counteracts the comparatively larger number of uniformly distributed sample points for later times when the current is changing much more slowly). The rate constants reported in Table 1 are the mean ± SEM for models optimized to data from individual oocytes; in each case, the optimized model was the result of globally fitting all of the data (I-V and Cole–Moore) for that oocyte.

RESULTS

A consistent effect of alanine substitutions among KCNH family members

hEAG1 channels produce a classic delayed rectifier current that saturates, or "rectifies," at higher voltages (Fig. 2, A and G; Robertson et al., 1996; Garg et al., 2012; Lörinczi et al., 2016). Like members of the other KCNH subfamilies that have been reported, hEAG1 channels possess a CNBhD in which the binding pocket is occupied by the intrinsic ligand (Fig. 1, A and B; Brelidze et al., 2012, 2013; Marques-Carvalho et al., 2012; Ng et al., 2013). Despite the remarkable similarity of the CNBhD structures, previous studies showed that human ERG1

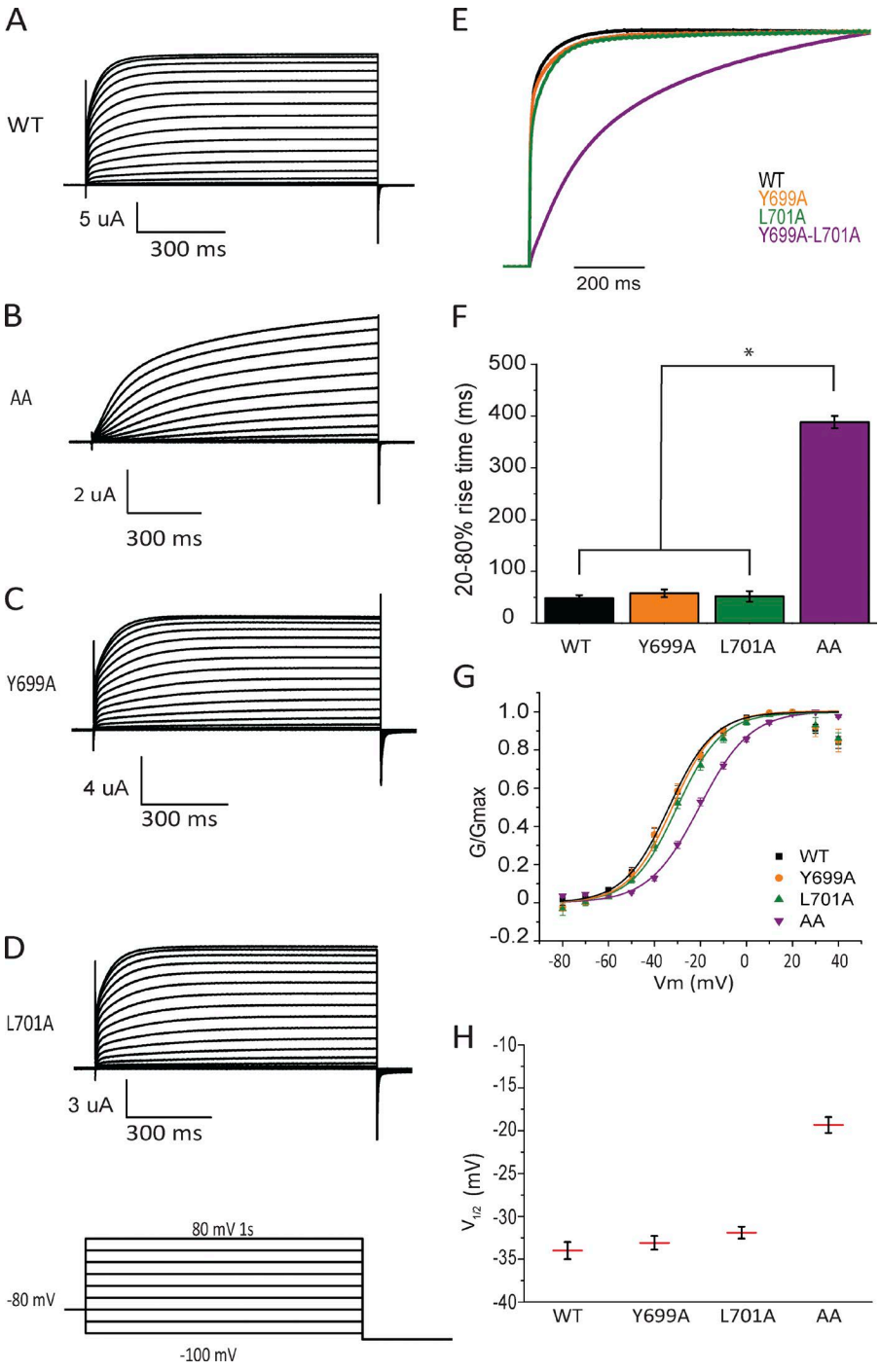

Figure 2. **The intrinsic ligand exerts a synergistic impact on hEAG1 channel gating.** Two-electrode voltage clamp current recorded from oocytes expressing WT (A), Y699A-L701A (B), Y699A (C), and L701A (D). All currents were recorded at room temperature in response to a series of 1-s depolarizing voltage steps ranging from −100 to 80 mV from a holding potential of −80 mV. (E) Overlaid normalized current traces of WT, Y699A, L701A, and Y699A-L701A. (F) Summary of 20–80% rise times for current activation at 60 mV (*, $P < 0.05$). (G) Normalized peak conductance (see Materials and methods) plotted as a function of test voltage. Data were fitted with a Boltzmann function (curves). (H) Summary of the $V_{1/2}$ from Boltzmann fits as shown in G. $n = 8$ (WT), 6 (Y699A-L701A), 5 (Y699A), and 7 (L701A) oocytes. Data are mean ± SEM.

and zebrafish ELK undergo positive G-V shifts in response to alanine mutagenesis of the intrinsic ligand (Brelidze et al., 2012, 2013), whereas the EAG1 G-V shifts to more negative potentials (Marques-Carvalho et al., 2012; Carlson et al., 2013). We repeated the analysis in hEAG1 and found that the AA mutation dramatically slowed activation relative to WT (Fig. 2, A, B, and E) and, in contrast to the previous study, conferred a positive shift in the G–V consistent with that in other KCNH family members (Fig. 2, G and H). Single alanine mutations in hEAG1 had little effect (Fig. 2, C–H), as previously reported (Marques-Carvalho et al., 2012). The cause of the discrepancy between EAG1 studies is not clear, but our study shows that the ligand-binding pocket interaction is not inherently different in hEAG1 channels and suggests that there is a consistent effect of the ligand interaction and its perturbation in all three KCNH subfamilies.

The channel gating machinery senses distinct ligation states of the CNBhD

Although the AA mutant was intended to mimic the removal of the intrinsic ligand by trimming the side

chains, alanine may nonetheless allow hydrophobic interactions with the binding pocket. Thus, we mutated the intrinsic ligand to double serine (SS) bearing a hydroxyl side chain and double glycine (GG) missing the β carbon and thus unable to interact with the binding pocket via side chains. Mutant channels were subjected to the same voltage protocol described earlier for alanine substitutions (Fig. 3, A–D). Compared with WT, both SS and GG impaired channel activation in a manner similar to that of AA by slowing current rise and shifting the G–V to more depolarized potentials, although to different extents. SS and GG slowed the 20–80% activation time at 60 mV by about threefold (Fig. 3, E and F) and shifted the G-V relation to the right by 30 and 40 mV, respectively (Fig. 3, G and H). Overall, all the tested double substitutions of the intrinsic ligand residues impeded channel activation, showing that the native CNBhD is critical for the rapid activation of the hEAG1 channel and impacts its voltage sensitivity. Furthermore, the differential effects of AA, SS, and GG substitutions indicate that the gating machinery is sensitive to multiple ligation states or conformations of the CNBhD.

Role of the CNBhD in activation steps preceding pore opening

Next, we tested the effect of eliminating the entire CNBhD by deleting residues 577–708 (ΔCNBhD; Fig. 1 A). Excising the CNBhD dramatically slowed channel activation (Fig. 4, A–E) and shifted the G-V relationship by 40 mV (Fig. 4, F and G). Interestingly, deleting the CNBhD resulted in behavior strikingly similar to that of the GG mutant in terms of both kinetics and voltage dependence, suggesting that the GG mutant is equivalent to the loss of the CNBhD.

To more stringently test the functional equivalence of the ΔCNBhD and GG mutants, we determined the effects of voltage prepulses from −130 mV to −20 mV on currents elicited by a test pulse at 60 mV immediately after the prepulse for WT, ΔCNBhD, and GG channels (Fig. 5, A–C). The time course of current rise during the test pulse depends on the distribution of closed states along the activation pathway occupied by the channel population during the prepulse, and thus represents an important test of the effect of perturbing early activation steps associated with voltage sensor movement (Cole and Moore, 1960; Bannister et al., 2005). For WT channels, the 20–80% current rise time during the test pulse was steeply dependent on prepulse potentials beginning at −100 mV and saturating at −60 mV (Fig. 5 D). The sensitivity of the current rise time to prepulse potentials was shifted for both ΔCNBhD and GG mutants to nearly identical extents, such that the effect of prepulse potential had yet to saturate at −20 mV.

These findings indicate that the native CNBhD shapes functional properties by promoting gating transitions associated with voltage sensor activation, before pore opening. Moreover, the equivalent impact of ΔCNBhD and GG on prepulse-dependent activation kinetics reinforces the conclusion that the loss of the intrinsic ligand (GG) is functionally equivalent to loss of the entire CNBhD.

Intrinsic ligand deletion

In an attempt to create a loss-of-function mutation for the intrinsic ligand itself, we excised the stretch of three residues comprising the ligand (699–701, ΔYNL). Exemplar traces from this mutant compared with WT show that the mutant current amplitudes and conductance saturated partway through the voltage excursion and then increased again at higher voltages (Fig. 6, A and B). The G–V relation correspondingly reveals at least two components that are positively shifted along the voltage axis to differing degrees relative to WT; they could be fitted with a double Boltzmann relation in which the $V_{1/2}$ of the second component is shifted by as much as 50 mV beyond the WT $V_{1/2}$ (Fig. 6, D and E). Substituting negatively charged aspartic acid (DD) for the intrinsic ligand resulted in a similar two-component G–V curve (Fig. 6, C and D). Thus, the ligand deletion unexpectedly does not phenocopy the loss of its receptor, i.e., the ΔCNBhD mutant. Perhaps the ΔYNL and DD mutants adopt two different conformations at the intrinsic ligand binding pocket: (a) a conformation exerting a moderate and predictable effect on the channel gating like other ligand substitutions (AA and SS; Fig. 6, D and E, first component), and (b) an unliganded conformation leading to a extreme shift of the G-V reminiscent of the ΔCNBhD mutant (Fig. 6, D and E, second component). These two components could arise either from two populations of channels, one in each conformation, or from channels that interconvert between conformations.

A computational model for CNBhD influence on hEAG1 gating

The CNBhD clearly shapes current properties, but assigning these effects to particular conformational states is not possible from simple inspection of current behavior. To assist in this task, and create a template for future studies, we first attempted to fit our data with a simple sequential scheme involving single-step activation of four independent VSDs followed by pore opening (Fig. S1 A). This model did not adequately describe the observed current kinetics or voltage dependence (Fig. S1 B), so we turned to a model in which each of four identical VSDs must undergo two independent and sequential gating transitions before the concerted opening of the channel pore (activation portion of the model in Fig. 7 A). This model describes both *Drosophila* Shaker and Eag channel gating and was previously constrained by ionic and gating currents for Eag (Zagotta et al., 1994;

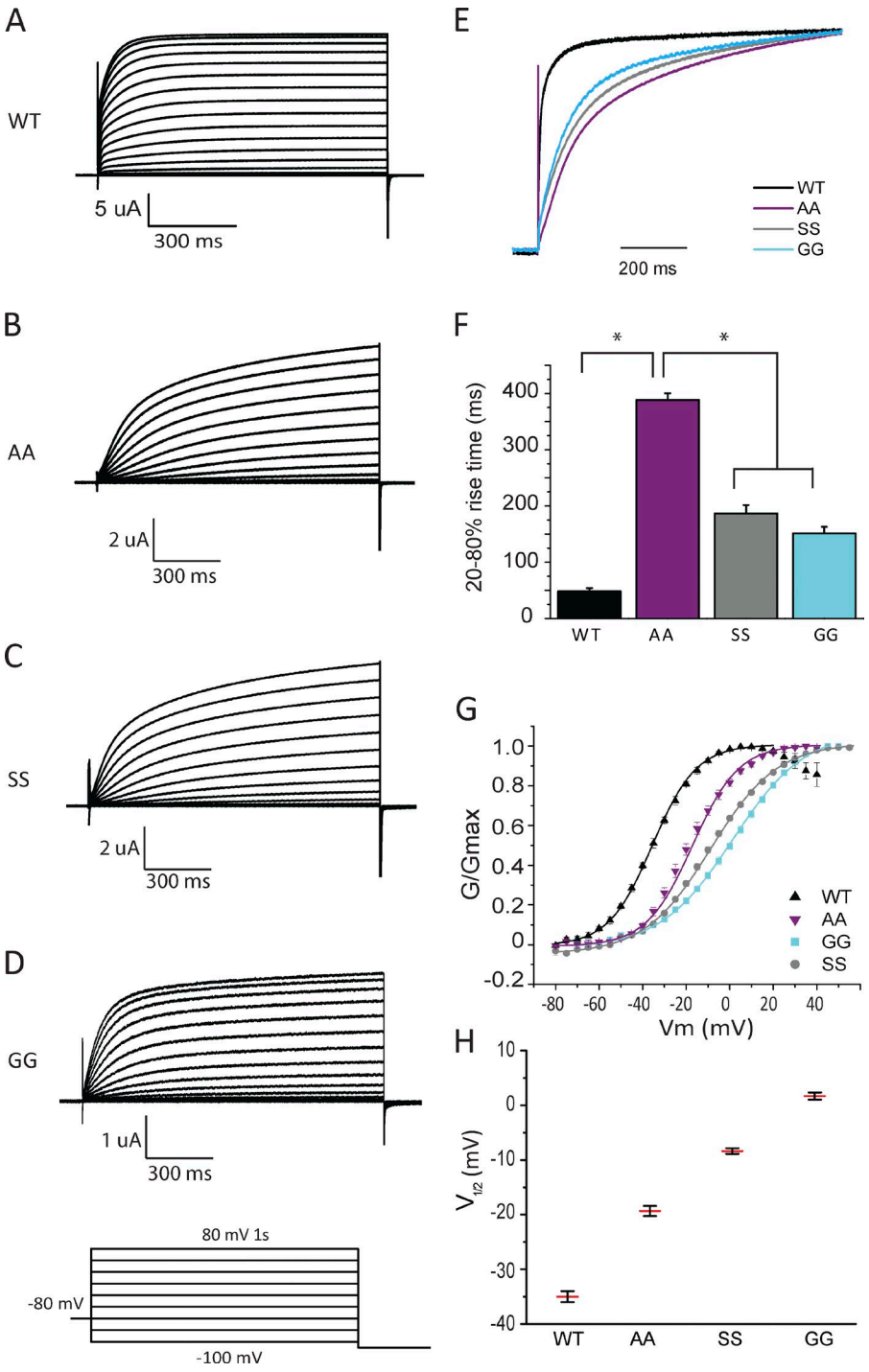

Figure 3. **The gating machinery senses different conformations of the CNBhD.** (A–D) Representative current traces evoked during 1-s voltage pulses ranging from −100 to 80 mV in 10-mV intervals from a holding potential of −80 mV for WT (A), AA (B), SS (C), and GG channels (D). (E) Overlaid normalized current responses at 60 mV. (F) Summary of 20–80% rise times for current activation at 60 mV (*, $P < 0.05$). (G) Normalized peak conductance plotted as a function of test voltage. Data were fitted with a Boltzmann function (see Materials and methods). (H) Summary of the $V_{1/2}$ derived from Boltzmann fits as shown in G. $n = 8$ (WT), 7 (AA), 8 (GG), and 6 (SS) oocytes. Data are mean ± SEM.

Tang et al., 2000). The model comprises intermediate states that correspond to the experimentally demonstrated stepwise rearrangements of two S4 arginines through a charge transfer center composed of hydrophobic and negatively charged residues (Silverman et al., 2003; Tao et al., 2010). Thus, we fixed the charge associated with each transition in the model to that determined in the previous Eag model (Tang et al., 2000).

A nonconducting state after the open state was required to fit the characteristic saturation observed at higher voltages (Fig. S2, A and B; Robertson et al., 1996; Garg et al., 2012; Lörinczi et al., 2016). We designated this state as "inactivated" (I) but do not imply mechanism, e.g., a true inactivated state versus Mg^{2+} block. Despite the additional free parameters this state adds to the model, it had little impact on the fits of activation kinetics and served only to scale the maximal current response (Fig. S2, C and D). Intriguingly, this model predicts a steady-state open probability at 40 mV of less than 0.5 (Fig. S2 G), sim-

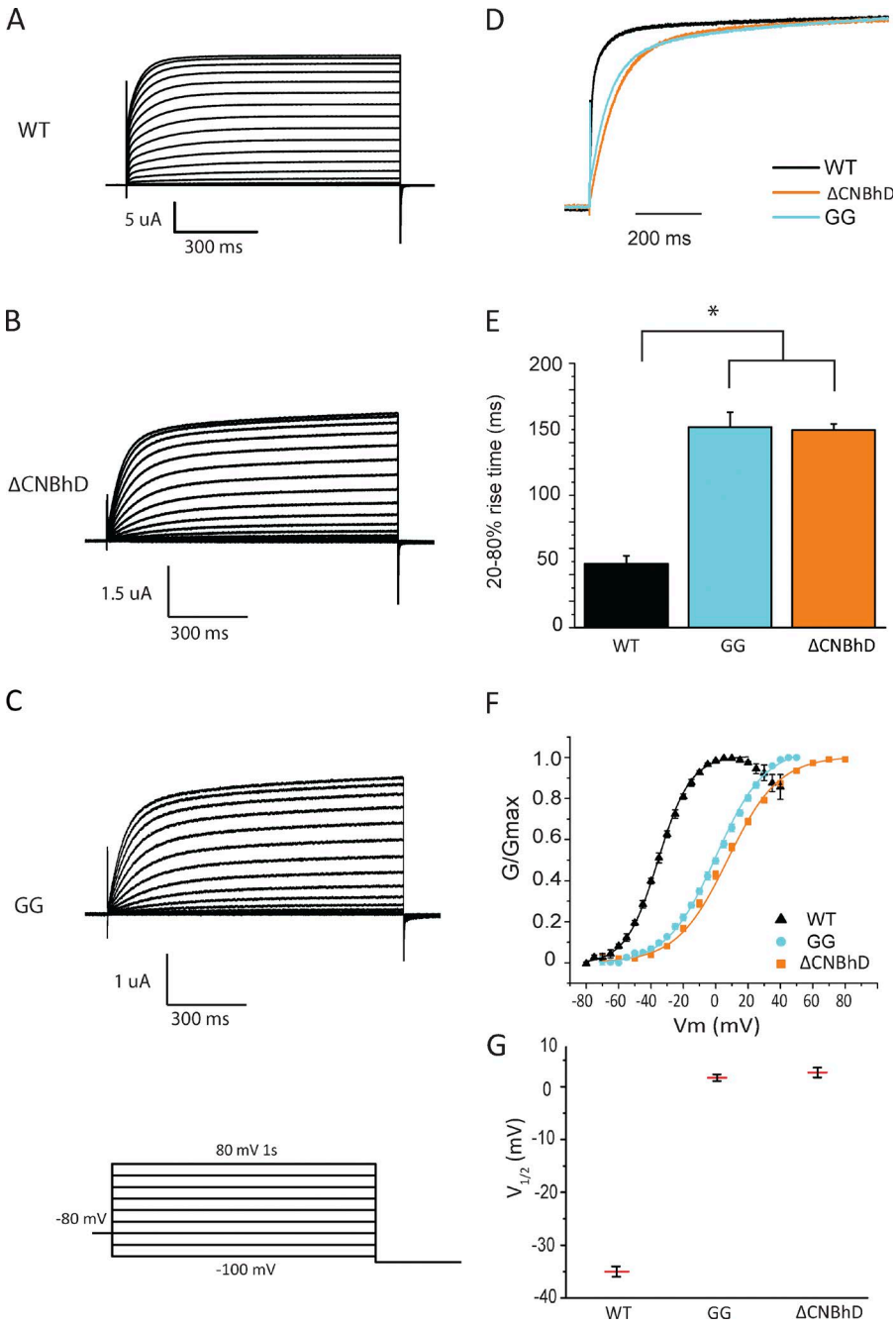

Figure 4. **GG mutant phenocopies CNBhD deletion.** (A–D) Representative current traces evoked during 1-s voltage pulses ranging from −100 to 80 mV in 10-mV intervals from a holding potential of −80 mV for WT (A), ΔCNBhD (B), and GG (C). (D) Overlaid normalized representative currents triggered at 60 mV. (E) Summary of 20–80% rise times for currents activated at 60 mV for WT and mutants (*, $P < 0.05$). (F) Normalized peak conductance plotted as a function of test voltage. Data were fitted with a Boltzmann function (see Materials and methods). (G) Summary of $V_{1/2}$ derived from Boltzmann fits for WT and the mutant channels. $n = 8$ (WT), 8 (GG), and 10 (ΔCNBhD) oocytes. Data are mean ± SEM.

ilar to that measured using nonstationary noise analysis (Ryan et al., 2012).

The WT model was optimized by simultaneously fitting to both current responses elicited by a range of depolarizing voltage steps from −100 to 80 mV (Fig. 7 B) and responses to a 60-mV step after a range of 1-s voltage prepulses from −130 to −20 mV (the Cole–Moore shift; Fig. 7 C). Simultaneous fits to multiple voltage protocols that stress different aspects of channel activation, including preopen closed states associated with movement of the voltage sensors, were important constraints during model optimization. Optimized rate constants (mean ± SEM) for models fitted to six oocytes are shown in Table 1.

After establishing a WT hEAG1 model, we next explored what aspects of the model had to be changed to account for the behavior of the ΔCNBhD mutant. For example, changing only rates associated with pore gating could not account for the slow sigmoidal activation of the ΔCNBhD mutant (Fig. S3 A). Altering only voltage sensor activation/deactivation rates similarly resulted in visually poor fits to the data (Fig. S3 B). In contrast, increasing the rate of pore closure and decreasing voltage sensor activation rates were sufficient to explain ΔCNBhD current responses to both I-V and prepulse protocols (Fig. 7, D and E). Model optimization was done as described for WT, except that rates

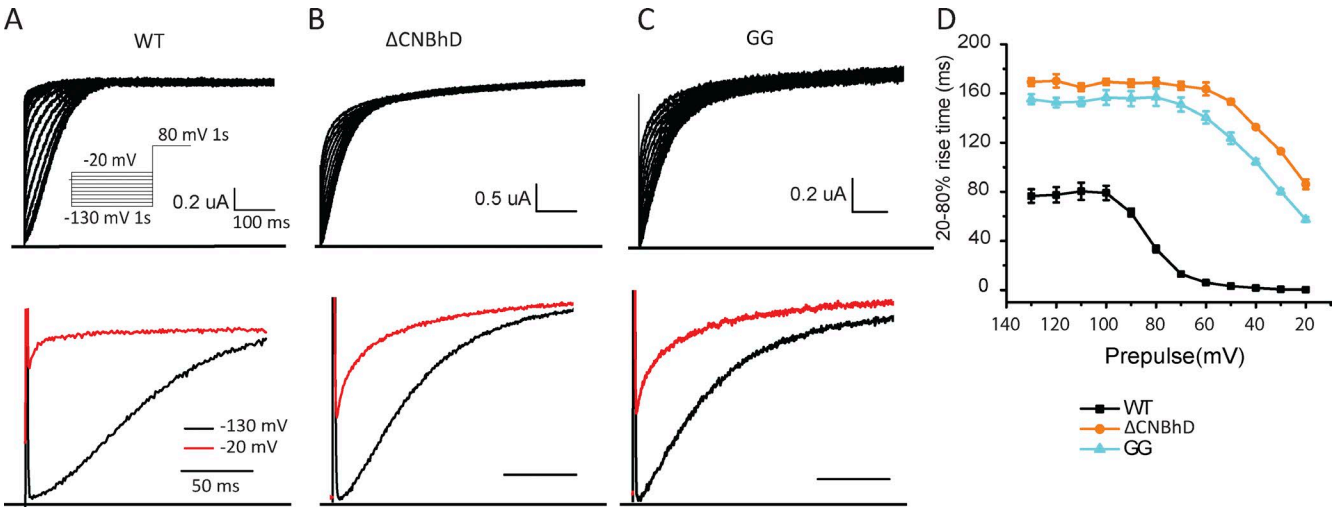

Figure 5. **GG and ΔCNBhD behave similarly in response to hyperpolarized prepulses.** Representative current traces triggered at 60 mV immediately after a series of voltage steps from −130 to −20 mV for WT (A), ΔCNBhD (B), and GG (C). (D) Normalized time of 20–80% maximum current at 60 mV plotted as a function of prepulse voltage for WT (black), ΔCNBhD (orange), and GG (cyan). *n* = 5 (WT), 7 (GG), and 4 (ΔCNBhD) oocytes. Data are mean ± SEM.

associated with pore opening and transitions to the inactivated state were fixed to their WT mean values. Although we cannot rule out a slowing of the pore opening rate, it was not necessary to explain the data, which nonetheless required changes in voltage sensor kinetics (Fig. S3 A). Optimized rate constants (mean ± SEM) for models fitted to six oocytes are shown in Table 1. Although current saturation was not obvious for the ΔCNBhD mutant, we left the inactivated state in the model for direct comparison with WT, and as for WT, there was no effect on ΔCNBhD activation kinetics (Fig. S2, E and F).

Comparison with the WT model suggests that removal of the CNBhD results in a destabilization of the open

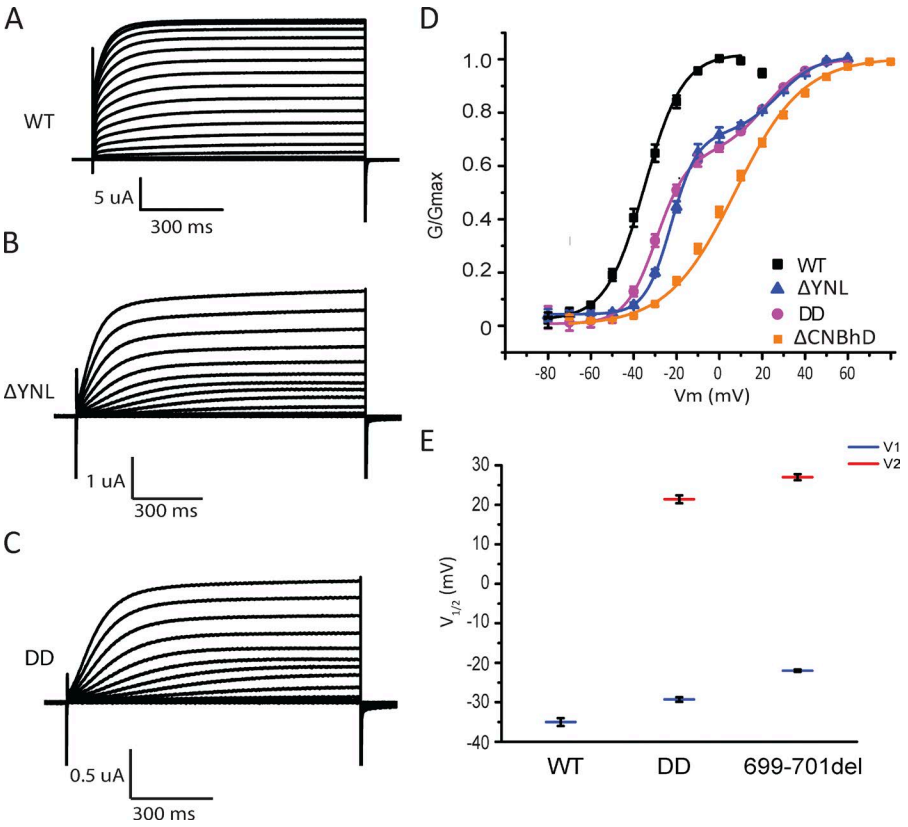

Figure 6. **ΔYNL intrinsic ligand deletion and DD mutant phenotypes.** (A–C) Representative current traces evoked during 1-s voltage pulses ranging from −100 to 80 mV in 10-mV intervals from a holding potential of −80 mV for WT (A), ΔYNL (B), and DD (C). (D) Normalized conductance plotted as a function of test voltage for WT, ΔYNL, and DD. WT was fitted with the single Boltzmann function (see Materials and methods). ΔYNL and DD were fitted with double Boltzmann function. (E) Summary of $V_{1/2}$ of WT and mutant channels. $V_{1/2}$ of the first Boltzmann component (V1) is indicated in blue, and the second component (V2) is in red. *n* = 8 (WT), 6 (DD), and 7 (ΔYNL) oocytes. Data are mean ± SEM.

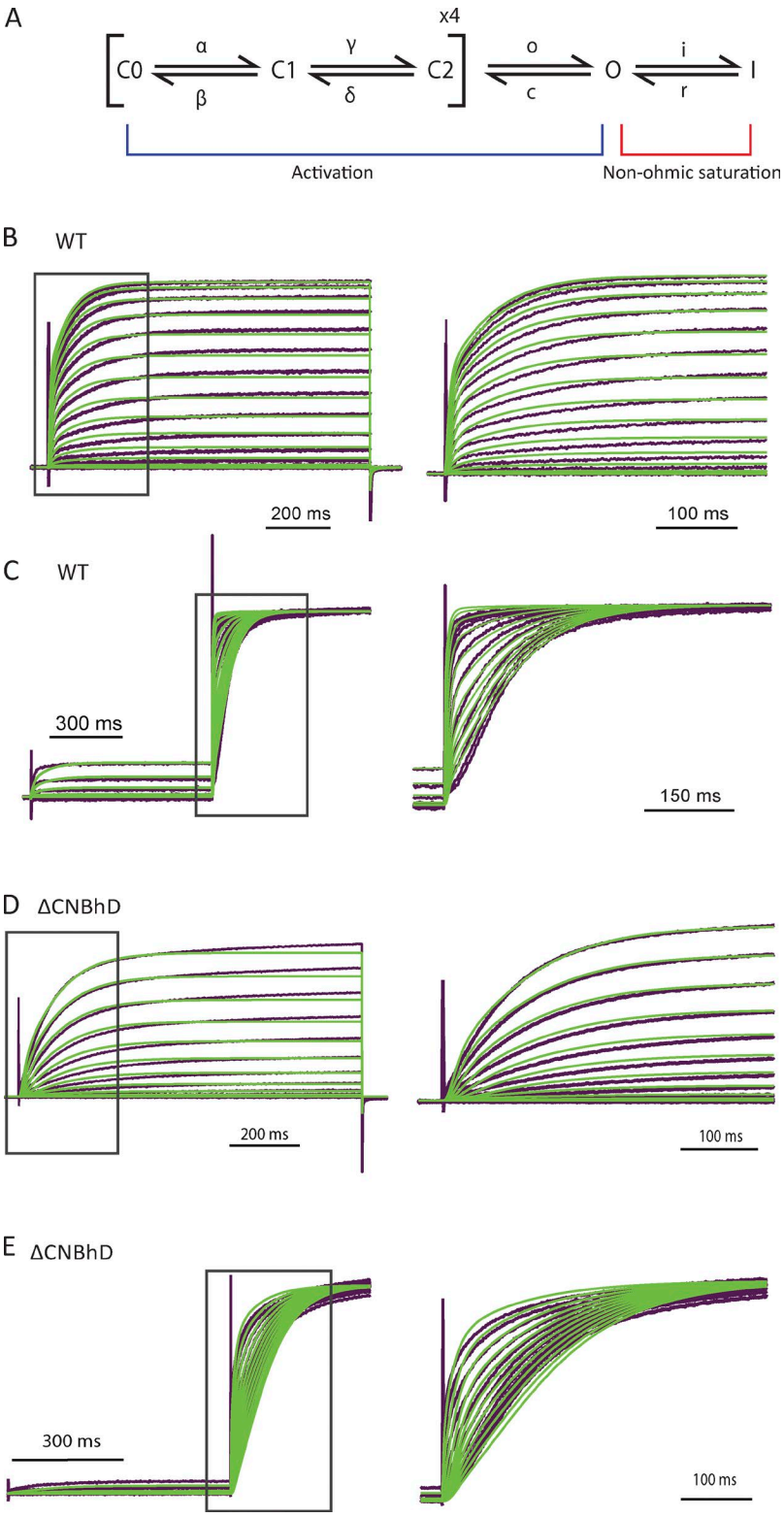

Figure 7. **Gating model for hEAG1 WT and ΔCNBhD channels.** (A) Kinetic model for channel gating. The bracketed transitions from C0 to C2 must proceed for each of four independent subunits before pore opening. The blue bracket indicates transitions that contribute to current activation kinetics. The red bracket indicates the transition that contributes to the nonohmic saturation at depolarized potentials (Fig. S2, A and B). Optimized rate constants and associated charges are listed in Table 1. (B, left) Representative currents from WT channels (purple) recorded in response to the protocol shown in Fig. 2 A, overlaid with simulated currents (green) from the model in A. (B, right) the initial 300 ms of the I-V recording shown on an expanded time scale. (C, left) Currents from WT channels (purple) recorded in response to the protocol shown in Fig. 5 A, overlaid with simulated currents (green). (C, right) The initial 350 ms of the Cole–Moore effect shown on an expanded time scale. (D and E) Representative currents from ΔCNBhD channels (purple), overlaid with simulated currents (green) in response to the same protocols shown in B and C, respectively.

pore as reflected by a 12-fold acceleration of the transition from O to C2. In addition, removal of the CNBhD slowed the transition between intermediate closed states along the activation pathway, thereby stabilizing the voltage sensors in conformations that are not fully activated. The enhanced occupancy of deep closed states explains not only the slow current activation kinetics, but also the Cole–Moore shift observations, in which more depolarized prepulses are needed to activate the ΔCNBhD mutant at rates approaching those of WT.

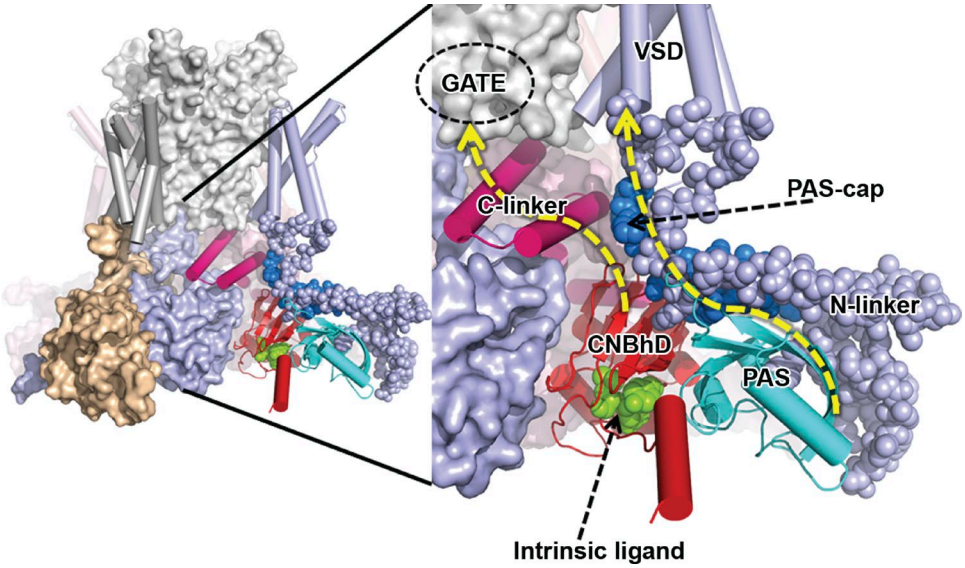

Figure 8. **Contacts in the cytoplasmic gating ring of EAG1.** Overall view of the EAG1 channel structure (PDB accession no. 5K7L) on the left with pore domain (gray surface) surrounded by voltage sensor domains (helical representation) at the top and the cytoplasmic gating ring at the bottom (as surface and cartoon representations). On the right, closer view of one of the units that form the cytoplasmic gating ring. The unit is assembled from the N terminus (PAS-cap, PAS domain, and N-linker, in shades of blue) of one channel subunit and the C terminus (C-linker and CNBhD, in shades of red) from another subunit. Domains and channel regions are labeled. Yellow arrows indicate putative pathways for propagation of structural changes affecting the gating mechanism, as discussed in the text.

DISCUSSION

Using mutagenesis and two-electrode voltage clamp, we explored the role of the CNBhD and its intrinsic ligand in the gating of the hEAG1 channel. We demonstrated that different conformations of the intrinsic ligand are communicated to the gating machinery with a range of effects. Substituting glycines for the liganding residues evoked phenotypes that closely matched the effects of the CNBhD deletion on both activation gating and the Cole–Moore shift, suggesting that the double GG mutation confers a complete loss of CNBhD function. Kinetic modeling suggests that CNBhD deletion selectively hastens pore closure and slows activation of the VSDs. These findings support a hypothesis in which the WT CNBhD promotes channel opening by stabilizing the open pore and promoting the fully activated conformation of the voltage sensors, thereby reducing barriers to channel opening in the activation pathway. The nearly identical effects conferred by the GG mutation and ΔCNBhD suggest that the intrinsic ligand is required for the CNBhD to exert these effects.

The KCNH family shares an ancestral relationship with HCN and cyclic nucleotide–gated ion channels reflected in the primary sequence of the CNBhD/CNBD and transmembrane regions (Warmke and Ganetzky, 1994; Ganetzky et al., 1999). Are the sequence similarities reflected in functional commonalities? Deleting the CNBD accelerates HCN1 and HCN2 activation (Barbuti et al., 1999; Wainger et al., 2001), whereas CNBhD deletion slows hEAG1 activation, suggesting prima facie an opposing effect. However, these apparently opposing effects can be explained by an analogous interaction by which the intact CNBD/CNBhD promotes the up or outward position of the S1–S4 VSDs: in the absence of the CNBD, the HCN1 VSD is more likely to be in the down position, promoting the opening of this hyperpolarization-activated channel (Vemana et al., 2004); in the absence of the CNBhD, the hEAG1 VSDs are also more likely to be in the down position, which, for hEAG1 channels, promotes channel closing. Our observation that deleting the CNBhD affects transitions early in the gating sequence, reported by the Cole–Moore shift previously demonstrated to reflect VSD movements (Bannister et al., 2005; Lörinczi et al., 2015), supports such a hypothesis.

Additional insights are gleaned by considering our results in light of the recent cryo-EM structure of the closely related rat EAG1 channel complexed with calmodulin (Fig. 8; Whicher and MacKinnon, 2016). The structure shows that the voltage sensor is in the activated or up position, whereas the pore gate is unexpectedly closed, possibly reflecting the inhibitory mechanism of calmodulin. Each of four CNBhDs interacts with the C-linker of the same subunit, providing a conduit for the effect of the CNBhD on the pore gate via its backbone connections with the C-linker (Fig. 8, left yellow arrow). Each CNBhD interacts with a Per-Arnt-Sim (PAS) domain of the neighboring subunit, consistent with previous functional and structural stud-

ies (Stevens et al., 2009; Gustina and Trudeau, 2011; Gianulis et al., 2013; Haitin et al., 2013; Ng et al., 2014). The PAS domain interacts with the VSD through the N-linker, the region between the PAS domain and the first transmembrane domain, and via the PAS cap. Thus, destabilizing the intrinsic ligand could lead to widespread changes in this gating ring by altering the position, orientation, or flexibility of not only the CNBhD and its associated C-linker, but also the interfacing PAS domain, PAS cap, and N-linker from the neighboring subunit (Fig. 8, right arrow). It is easy to imagine that these changes could be directly conveyed to the pore gate and the VSD.

Our data indicate that different conformations of the CNBhD, conferred by different mutations of the intrinsic ligand, can be detected by the gating machinery. Interestingly, for the HCN channel, it has been shown in vitro that the integrity of the gating ring is dependent on the occupancy of the nucleotide-binding pocket (Lolicato et al., 2011). Specifically, in the unbound state, the stability of the tetrameric C-linker/CNBD assembly is reduced and the monomeric form predominates. Perhaps our different mutations of the intrinsic ligand in the EAG1 channel affect the gating assembly in a similar manner so that in the extreme case of the GG mutant, there is a disruption of the gating ring tetrameric structure analogous to that of the unliganded HCN channel.

In summary, our computational model faithfully replicates hEAG1 current kinetics over a wide voltage range and also accounts for the observed Cole–Moore shift in activation kinetics after voltage prepulses. The model, together with our experimental findings, shows that removal of either the CNBhD (ΔCNBhD) or its intrinsic ligand (GG) destabilizes the open pore and slows activation of the voltage sensors. Thus, the role of the intact intrinsically liganded CNBhD is to both stabilize the open pore and promote the fully activated conformation of the voltage sensors. Collectively, our observations and models advance our understanding of the influence of the CNBhD on channel gating and provide a basis for future studies of the mechanism underlying these interactions.

ACKNOWLEDGMENTS

We thank Dr. Roland Schonherr for providing the hEAG1 plasmid and Dr. Phu Tran and Colin Peters for providing preliminary data. We thank current members of the Robertson laboratory for helpful discussions.

This work was supported by National Institutes of Health grants NS081320 (to G.A. Robertson and J.H. Morais-Cabral) and NS081293 (to B. Chanda).

The authors declare no competing financial interests.

Sharona E. Gordon served as editor.

Submitted: 29 September 2016
Revised: 29 November 2016
Accepted: 21 December 2016

REFERENCES

Bannister, J.P., B. Chanda, F. Bezanilla, and D.M. Papazian. 2005. Optical detection of rate-determining ion-modulated conformational changes of the ether-à-go-go K+ channel voltage sensor. *Proc. Natl. Acad. Sci. USA.* 102:18718–18723. http://dx.doi.org/10.1073/pnas.0505766102

Barbuti, A., M. Baruscotti, C. Altomare, A. Moroni, and D. DiFrancesco. 1999. Action of internal pronase on the f-channel kinetics in the rabbit SA node. *J. Physiol.* 520:737–744. http://dx.doi.org/10.1111/j.1469-7793.1999.00737.x

Brelidze, T.I., A.E. Carlson, and W.N. Zagotta. 2009. Absence of direct cyclic nucleotide modulation of mEAG1 and hERG1 channels revealed with fluorescence and electrophysiological methods. *J. Biol. Chem.* 284:27989–27997. http://dx.doi.org/10.1074/jbc.M109.016337

Brelidze, T.I., A.E. Carlson, B. Sankaran, and W.N. Zagotta. 2012. Structure of the carboxy-terminal region of a KCNH channel. *Nature.* 481:530–533. http://dx.doi.org/10.1038/nature10735

Brelidze, T.I., E.C. Gianulis, F. DiMaio, M.C. Trudeau, and W.N. Zagotta. 2013. Structure of the C-terminal region of an ERG channel and functional implications. *Proc. Natl. Acad. Sci. USA.* 110:11648–11653. http://dx.doi.org/10.1073/pnas.1306887110

Carlson, A.E., T.I. Brelidze, and W.N. Zagotta. 2013. Flavonoid regulation of EAG1 channels. *J. Gen. Physiol.* 141:347–358. http://dx.doi.org/10.1085/jgp.201210900

Clayton, G.M., W.R. Silverman, L. Heginbotham, and J.H. Morais-Cabral. 2004. Structural basis of ligand activation in a cyclic nucleotide regulated potassium channel. *Cell.* 119:615–627. http://dx.doi.org/10.1016/j.cell.2004.10.030

Cole, K.S., and J.W. Moore. 1960. Ionic current measurements in the squid giant axon membrane. *J. Gen. Physiol.* 44:123–167. http://dx.doi.org/10.1085/jgp.44.1.123

Ganetzky, B., G.A. Robertson, G.F. Wilson, M.C. Trudeau, and S.A. Titus. 1999. The eag family of K+ channels in *Drosophila* and mammals. *Ann. N. Y. Acad. Sci.* 868(1 MOLECULAR AND):356–369. http://dx.doi.org/10.1111/j.1749-6632.1999.tb11297.x

Garg, V., F.B. Sachse, and M.C. Sanguinetti. 2012. Tuning of EAG K^+ channel inactivation: Molecular determinants of amplification by mutations and a small molecule. *J. Gen. Physiol.* 140:307–324. http://dx.doi.org/10.1085/jgp.201210826

Gianulis, E.C., Q. Liu, and M.C. Trudeau. 2013. Direct interaction of eag domains and cyclic nucleotide-binding homology domains regulate deactivation gating in hERG channels. *J. Gen. Physiol.* 142:351–366. http://dx.doi.org/10.1085/jgp.201310995

Goldschen-Ohm, M.P., A. Haroldson, M.V. Jones, and R.A. Pearce. 2014. A nonequilibrium binary elements-based kinetic model for benzodiazepine regulation of GABAA receptors. *J. Gen. Physiol.* 144:27–39. http://dx.doi.org/10.1085/jgp.201411183

Gustina, A.S., and M.C. Trudeau. 2011. hERG potassium channel gating is mediated by N- and C-terminal region interactions. *J. Gen. Physiol.* 137:315–325. http://dx.doi.org/10.1085/jgp.201010582

Guy, H.R., S.R. Durell, J. Warmke, R. Drysdale, and B. Ganetzky. 1991. Similarities in amino acid sequences of *Drosophila eag* and cyclic nucleotide-gated channels. *Science.* 254:730. http://dx.doi.org/10.1126/science.1658932

Haitin, Y., A.E. Carlson, and W.N. Zagotta. 2013. The structural mechanism of KCNH-channel regulation by the eag domain. *Nature.* 501:444–448. http://dx.doi.org/10.1038/nature12487

Hodgkin, A.L., and B. Katz. 1949. The effect of sodium ions on the electrical activity of giant axon of the squid. *J. Physiol.* 108:37–77. http://dx.doi.org/10.1113/jphysiol.1949.sp004310

Kortüm, F., V. Caputo, C.K. Bauer, L. Stella, A. Ciolfi, M. Alawi, G. Bocchinfuso, E. Flex, S. Paolacci, M.L. Dentici, et al. 2015.

Mutations in KCNH1 and ATP6V1B2 cause Zimmermann-Laband syndrome. *Nat. Genet.* 47:661–667. http://dx.doi.org/10.1038/ng.3282

Lolicato, M., M. Nardini, S. Gazzarrini, S. Möller, D. Bertinetti, F.W. Herberg, M. Bolognesi, H. Martin, M. Fasolini, J.A. Bertrand, et al. 2011. Tetramerization dynamics of C-terminal domain underlies isoform-specific cAMP gating in hyperpolarization-activated cyclic nucleotide-gated channels. *J. Biol. Chem.* 286:44811–44820. http://dx.doi.org/10.1074/jbc.M111.297606

Lörinczi, E., M. Helliwell, A. Finch, P.J. Stansfeld, N.W. Davies, M. Mahaut-Smith, F.W. Muskett, and J.S. Mitcheson. 2016. Calmodulin regulates human ether à go-go 1 (hEAG1) potassium channels through interactions of the eag domain with the cyclic nucleotide binding homology domain. *J. Biol. Chem.* 291:17907–17918. http://dx.doi.org/10.1074/jbc.M116.733576

Lörinczi, É., J.C. Gómez-Posada, P. de la Peña, A.P. Tomczak, J. Fernández-Trillo, U. Leipscher, W. Stühmer, F. Barros, and L.A. Pardo. 2015. Voltage-dependent gating of KCNH potassium channels lacking a covalent link between voltage-sensing and pore domains. *Nat. Commun.* 6:6672. http://dx.doi.org/10.1038/ncomms7672

Ludwig, J., H. Terlau, F. Wunder, A. Brüggemann, L.A. Pardo, A. Marquardt, W. Stühmer, and O. Pongs. 1994. Functional expression of a rat homologue of the voltage gated either á go-go potassium channel reveals differences in selectivity and activation kinetics between the *Drosophila* channel and its mammalian counterpart. *EMBO J.* 13:4451–4458.

Marques-Carvalho, M.J., N. Sahoo, F.W. Muskett, R.S. Vieira-Pires, G. Gabant, M. Cadene, R. Schönherr, and J.H. Morais-Cabral. 2012. Structural, biochemical, and functional characterization of the cyclic nucleotide binding homology domain from the mouse EAG1 potassium channel. *J. Mol. Biol.* 423:34–46. http://dx.doi.org/10.1016/j.jmb.2012.06.025

Meyer, R., and S.H. Heinemann. 1998. Characterization of an eag-like potassium channel in human neuroblastoma cells. *J. Physiol.* 508:49–56. http://dx.doi.org/10.1111/j.1469-7793.1998.049br.x

Mortensen, L.S., H. Schmidt, Z. Farsi, A. Barrantes-Freer, M.E. Rubio, R. Ufartes, J. Eilers, T. Sakaba, W. Stühmer, and L.A. Pardo. 2015. KV 10.1 opposes activity-dependent increase in Ca2+ influx into the presynaptic terminal of the parallel fibre-Purkinje cell synapse. *J. Physiol.* 593:181–196. http://dx.doi.org/10.1113/jphysiol.2014.281600

Ng, C.A., Y. Ke, M.D. Perry, P.S. Tan, A.P. Hill, and J.I. Vandenberg. 2013. C-terminal β9-strand of the cyclic nucleotide-binding homology domain stabilizes activated states of Kv11.1 channels. *PLoS One.* 8:e77032. http://dx.doi.org/10.1371/journal.pone.0077032

Ng, C.A., K. Phan, A.P. Hill, J.I. Vandenberg, and M.D. Perry. 2014. Multiple interactions between cytoplasmic domains regulate slow deactivation of Kv11.1 channels. *J. Biol. Chem.* 289:25822–25832. http://dx.doi.org/10.1074/jbc.M114.558379

Pardo, L.A., D. del Camino, A. Sánchez, F. Alves, A. Brüggemann, S. Beckh, and W. Stühmer. 1999. Oncogenic potential of EAG K(+) channels. *EMBO J.* 18:5540–5547. http://dx.doi.org/10.1093/emboj/18.20.5540

Robertson, G.A., J.M. Warmke, and B. Ganetzky. 1996. Potassium currents expressed from *Drosophila* and mouse eag cDNAs in *Xenopus* oocytes. *Neuropharmacology.* 35:841–850. http://dx.doi.org/10.1016/0028-3908(96)00113-X

Ryan, M.Y., R. Maloney, J.D. Fineberg, R.A. Reenan, and R. Horn. 2012. RNA editing in *eag* potassium channels: Biophysical consequences of editing a conserved S6 residue. *Channels (Austin).* 6:443–452. http://dx.doi.org/10.4161/chan.22314

Sánchez, A., D. Urrego, and L.A. Pardo. 2016. Cyclic expression of the voltage-gated potassium channel KV10.1 promotes disassembly of the primary cilium. *EMBO Rep.* 17:708–723. http://dx.doi.org/10.15252/embr.201541082

Schönherr, R., G. Gessner, K. Löber, and S.H. Heinemann. 2002. Functional distinction of human EAG1 and EAG2 potassium channels. *FEBS Lett.* 514:204–208. http://dx.doi.org/10.1016/S0014-5793(02)02365-7

Silverman, W.R., B. Roux, and D.M. Papazian. 2003. Structural basis of two-stage voltage-dependent activation in K+ channels. *Proc. Natl. Acad. Sci. USA.* 100:2935–2940. http://dx.doi.org/10.1073/pnas.0636603100

Simons, C., L.D. Rash, J. Crawford, L. Ma, B. Cristofori-Armstrong, D. Miller, K. Ru, G.J. Baillie, Y. Alanay, A. Jacquinet, et al. 2015. Mutations in the voltage-gated potassium channel gene KCNH1 cause Temple-Baraitser syndrome and epilepsy. *Nat. Genet.* 47:73–77. http://dx.doi.org/10.1038/ng.3153

Stevens, L., M. Ju, and D. Wray. 2009. Roles of surface residues of intracellular domains of heag potassium channels. *Eur. Biophys. J.* 38:523–532. http://dx.doi.org/10.1007/s00249-009-0402-8

Tang, C.Y., F. Bezanilla, and D.M. Papazian. 2000. Extracellular Mg^{2+} modulates slow gating transitions and the opening of *Drosophila* ether-à-Go-Go potassium channels. *J. Gen. Physiol.* 115:319–338. http://dx.doi.org/10.1085/jgp.115.3.319

Tao, X., A. Lee, W. Limapichat, D.A. Dougherty, and R. MacKinnon. 2010. A gating charge transfer center in voltage sensors. *Science.* 328:67–73. http://dx.doi.org/10.1126/science.1185954

Vemana, S., S. Pandey, and H.P. Larsson. 2004. S4 movement in a mammalian HCN channel. *J. Gen. Physiol.* 123:21–32. http://dx.doi.org/10.1085/jgp.200308916

Wainger, B.J., M. DeGennaro, B. Santoro, S.A. Siegelbaum, and G.R. Tibbs. 2001. Molecular mechanism of cAMP modulation of HCN pacemaker channels. *Nature.* 411:805–810. http://dx.doi.org/10.1038/35081088

Warmke, J.W., and B. Ganetzky. 1994. A family of potassium channel genes related to eag in *Drosophila* and mammals. *Proc. Natl. Acad. Sci. USA.* 91:3438–3442. http://dx.doi.org/10.1073/pnas.91.8.3438

Warmke, J., R. Drysdale, and B. Ganetzky. 1991. A distinct potassium channel polypeptide encoded by the *Drosophila* eag locus. *Science.* 252:1560–1562. http://dx.doi.org/10.1126/science.1840699

Whicher, J.R., and R. MacKinnon. 2016. Structure of the voltage-gated K^+ channel Eag1 reveals an alternative voltage sensing mechanism. *Science.* 353:664–669. http://dx.doi.org/10.1126/science.aaf8070

Wu, C.F., B. Ganetzky, F.N. Haugland, and A.X. Liu. 1983. Potassium currents in *Drosophila*: Different components affected by mutations of two genes. *Science.* 220:1076–1078. http://dx.doi.org/10.1126/science.6302847

Zagotta, W.N., T. Hoshi, and R.W. Aldrich. 1994. Shaker potassium channel gating. III: Evaluation of kinetic models for activation. *J. Gen. Physiol.* 103:321–362. http://dx.doi.org/10.1085/jgp.103.2.321

Zagotta, W.N., N.B. Olivier, K.D. Black, E.C. Young, R. Olson, and E. Gouaux. 2003. Structural basis for modulation and agonist specificity of HCN pacemaker channels. *Nature.* 425:200–205. http://dx.doi.org/10.1038/nature01922